3-2007

Energy Release Characteristics of The Nanoscale Aluminum-Tungsten Oxide Hydrate Metastable Intermolecular Composite

W. Lee Perry
Los Alamos National Laboratory, wperry@lanl.gov

Bryce C. Tappan
Los Alamos National Laboratory

Bettina L. Reardon
Los Alamos National Laboratory

Victor E. Sanders
Los Alamos National Laboratory

Steven F. Son
Los Alamos National Laboratory

Recommended Citation
W. L. Perry, B. C. Tappan, B. L. Smith, V. E. Sanders, and S. F. Son, "Energy release characteristics of the nano-scale aluminum tungsten-oxide hydrate metastable intermolecular composite," Journal of Applied Physics, 101(6): 064313, 2007. dx.doi.org/10.1063/1.2435797

Energy release characteristics of the nanoscale aluminum-tungsten oxide hydrate metastable intermolecular composite

W. Lee Perry, Bryce C. Tappan, Bettina L. Reardon, Victor E. Sanders, and Steven F. Son

Citation: Journal of Applied Physics **101**, 064313 (2007);
View online: https://doi.org/10.1063/1.2435797
View Table of Contents: http://aip.scitation.org/toc/jap/101/6
Published by the American Institute of Physics

Energy release characteristics of the nanoscale aluminum-tungsten oxide hydrate metastable intermolecular composite

W. Lee Perry,[a] Bryce C. Tappan, Bettina L. Reardon, Victor E. Sanders, and Steven F. Son
Dynamic Experimentation Division, Los Alamos National Laboratory, Los Alamos, New Mexico 87545

(Received 20 July 2006; accepted 11 December 2006; published online 26 March 2007)

Tungsten oxides are of interest as an oxidant for metals in metastable intermolecular composites (MICs), a reactive nanoscale powder useful for such applications as electric matches and gun primers. Smaller particles typically lead to fast reaction rates in this class of energetic material, and we have synthesized nanoscale $WO_3 \cdot H_2O$ using wet chemistry. Analysis by electron microscopy and small angle x-ray scattering revealed an approximately 100-nm-wide by 7-nm-thick platelet morphology. X-ray diffraction verified the orthorhombic structure and composition of the hydrate. A MIC material was formulated using 44 nm Al as the fuel. Performance was measured using a pressure cell where total enthalpy change and energy release rate was measured. This report includes the thermodynamic analysis of the pressure cell (calorimetry) that allows the determination of these metrics. Accuracy of the technique is discussed. Performance of the hydrate was found to significantly exceed that of MIC formulated with dehydrated tungsten oxide for one formulation, having an energy release of approximately 1.8 MJ/kg at a rate of approximately 215 GW/m^2, compared to around 1.1 MJ/kg at a rate of around 130 GW/m^2 for the dehydrated formulation. The data show that the enhanced behavior of the hydrated MIC formulation resulted from the reaction of aluminum with the interstitially bound water, which had additional energy release and generated hydrogen gas. © *2007 American Institute of Physics*. [DOI: 10.1063/1.2435797]

INTRODUCTION

Metastable intermolecular composite (MIC) materials are an advancement of conventional thermites. Aumann *et al.* provided an early report of MIC materials and a good conceptual description of their reactivity.[1] In short, the application of nanotechnology leads to a thermite having ultrafine particle sizes and reduced heat and mass transfer length scales, leading to significantly higher energy release rates relative to conventional thermites. Also, thermites typically have an energy density that exceeds that of conventional energetic materials[2,3] and release the energy at a rate on the order of 100 GW/m^2 of combustion front.[2,4] Typical MIC reactions are explosive in nature and, for comparison, detonation produces energy on the order of 50 TW/m^2. MIC systems have a distinct advantage by providing flexibility in energy density and power through control of particle size distribution, stoichiometry, and choice of fuel and oxidizer. MICs and ultrafine powders have found applications in primers,[5] electric matches,[6] and explosives.[7,8]

The use of nanoscale tungsten oxides is of interest as a MIC oxidizer. The material finds advantages for such applications as environmentally friendly electric matches and gun primers by maintaining good performance without the use of lead. High performance MIC materials of nanosized WO_3 and 44 nm Al have recently been demonstrated. This previous work has shown that the propagation velocity for these MIC materials can reach 250 m/s with an energy density of 1.1 MJ/kg and a maximum energy release rate of around 130 GW/m^2. These values were obtained with an experimentally determined optimal stoichiometric O/Al molar ratio near 1.5.[9]

The procedure used for generating the nano-WO_3 produced $WO_3 \cdot H_2O$, which was subsequently annealed to remove the water. Our previous research detailed the synthesis process, the dehydration procedure, and the resulting oxide material.[9] Initial performance studies indicated that formulation of a MIC with the hydrated tungsten oxide had a very high energy release rate. We hypothesized that the presence of structural water in the oxidizer may influence the performance of MIC, and we report here a study comparing the hydrate performance to that of oxide, and the performance of both to the behavior expected from thermodynamic calculations. The evidence presented here suggested that water participated reactively, adding energy to the system, and produced hydrogen gas.

EXPERIMENT

$WO_3 \cdot H_2O$ was formed through the previously described crash precipitation method.[9] Briefly, the method involved dissolving ammonium paratungstate in acid to form tungstic acid. Tungsten oxide hydrate precipitated upon addition of distilled water and the resulting powder heated at 100 °C overnight in air. This method produces $WO_3 \cdot H_2O$ with particles that typically have a platelet morphology and ~100-nm-wide by 7-nm-thick particle sizes.

$WO_3 \cdot H_2O$/Al MIC materials were made using the previously described method.[9] The $WO_3 \cdot H_2O$ was placed in

[a]Author to whom correspondence should be addressed; FAX: 505-667-0500; electronic mail: wperry@lanl.gov

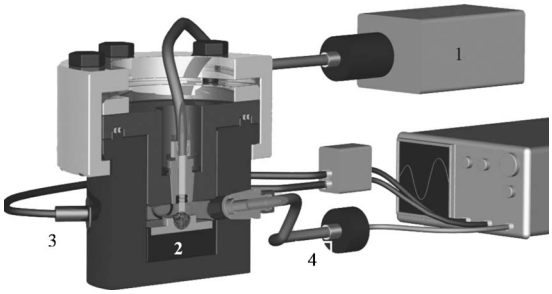

FIG. 1. Schematic of pressure cell diagnostic. Laser, via light fiber, ignites the material near the center of the cell. Transducers located radially and in plane with the sample record pressure and light output. The components include (1) laser, (2) sample, (3) pressure transducer, and (4) light fiber.

10 ml of isopropyl alcohol. This mixture was sonified for 10 min at which point 44 nm Al was added. The mixture of $WO_3 \cdot H_2O$/Al in isopropyl alcohol was again sonified for 30 s. After this final sonification, the sample was poured into a heated dish to evaporate the isopropyl alcohol. The dried MIC material was then gently brushed through a mesh material to form a fine powder. This material was mixed based on O/Al mole ratios of 1.1–2.1. The Al fuel employed in these experiments has an inert passivating oxide layer, accounting for 33% of the total mass. The mass ratios of $Al/WO_3 \cdot H_2O$, determined using the mole fraction and the oxide fraction, were 0.32–0.48.

The MIC material was performance tested through measurements of the pressure-time characteristics in a bomb apparatus (pressure cell). In these tests, the MIC material was placed into the pressure cell and initiated with a 30 ns 20 mJ/cm^2 Nd:YAG (yttrium aluminum garnet) laser pulse. The laser pulse triggers an oscilloscope that records the rate of pressurization through two pressure transducers (PCB Piezotronics Inc.). Voltage data were captured digitally using a Tektronix 460A oscilloscope. The data were recorded at a resolution of 100 ns/point for 50 000 points to ensure that the maximum pressure was obtained. Figure 1 shows a rendering of the apparatus.

A Netzsch STA 449 Jupiter provided the TGA-DSC data. This instrument was set to heat from ambient temperature to 900 °C at a rate of 10 °C/min. X-ray diffraction (XRD) was run using powder diffraction techniques. The scanning parameters for this instrument were set to scan from 5° to 80° with a step size of 0.05° per step and a rate of 3° per minute.

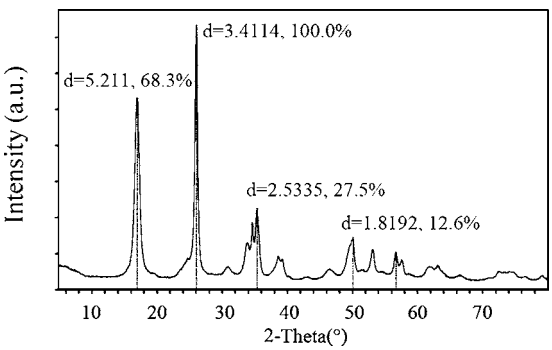

FIG. 2. X-ray diffraction pattern for orthorhombic $WO_3 \cdot H_2O$ from the crash precipitation method.

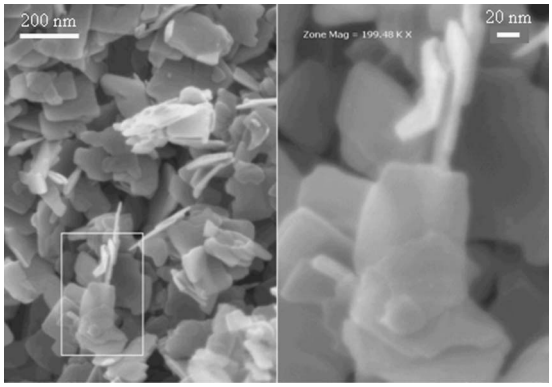

FIG. 3. Electron micrograph of $WO_3 \cdot H_2O$ produced by the crash precipitation method.

RESULTS AND DISCUSSION

We provide here evidence of the hydrate material's physical structure, morphology, and energy required for dehydration. A discussion of reaction thermodynamics follows, including an estimate of the accuracy of our calorimetric method. Finally, we compare the performance of a MIC formulated with the hydrate to a MIC formulated with the oxide, and the possible mechanistic differences between the two reactions.

Material characterization

The synthesis procedure produced pure orthorhombic $WO_3 \cdot H_2O$, as confirmed by several characterization techniques. Figure 2 shows a diffraction pattern from the material, showing the orthorhombic structure as referenced to the work of other researchers and to the International Center for Diffraction Data PDF file.[10,11] Figure 3 shows an electron microscope image of the material, revealing a platelet morphology. Rough particle sizing using scanning electron microscope images indicated a particle width of approximately 100 nm, and small angle x-ray scattering quantitatively found a particle thickness of 7 ± 0.2 nm.[12,13] Thermogravimetric analysis (TGA) analysis showed a mass loss consistent with that expected for $WO_3 \cdot H_2O \rightarrow WO_3$, as shown in Fig. 4. Differential scanning calorimetry (DSC) analysis, also

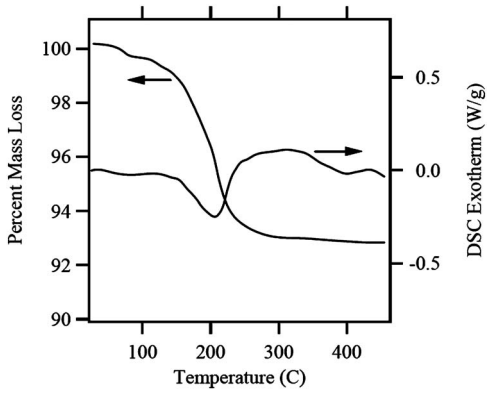

FIG. 4. TGA and DSC data showing the dehydration of $WO_3 \cdot H_2O$. The mass loss was approximately 6%, consistent with the loss of 1 mol of water for each mole of WO_3. The endotherm shown in the DSC data near 200 °C indicated 80–100 J/g of hydrate was required to remove the water.

shown in Fig. 4, shows the endothermic loss of water in the range of 190–250 °C, requiring approximately 80–100 J/g of hydrate to liberate the water.

Reaction thermodynamics

We have determined reaction enthalpies by a first law analysis of the pressure cell. The analysis begins with the basic form of the first law,

$$Q + W = \Delta U, \tag{1}$$

where Q is the heat exchanged with the surroundings and W is the work. The walls of the vessel do not move such that no work is done, and $W=0$. U is the total internal energy of the gas within the boundary of the vessel and Δ, as usual, refers to the general change that occurs from an initial state (1) to the state of interest (2). By definition U depends on enthalpy (H) and pressure (P) within the system,

$$Q = \Delta U = \Delta H - \Delta PV, \tag{2}$$

where V is the volume (constant) of the system. The total enthalpy change comprises reaction enthalpy, phase change enthalpy, and sensible heat enthalpy,

$$\Delta H = \Delta H^0_{\mathrm{rxn}} + \Delta H_{\mathrm{pc}} + \Delta H_{\mathrm{sens}}, \tag{3}$$

where the subscripts rxn, pc, and sens, refer to reaction, phase change, and sensible heat, respectively. The superscript "0" refers to the reference temperature, assumed here to be 298 K. The following familiar relationship replaces the sensible heat enthalpy:

$$\Delta H_{\mathrm{sens}} = n_2 C_{\mathrm{p}2} T_2 - n_1 C_{\mathrm{p}1} T_1. \tag{4}$$

n, C_p, and T refer to the molar amount of gas, constant-pressure heat capacity, and temperature. At state 2, the gas was a mixture of vapor products and heated air. At state 1, the gas was only air at ambient conditions. The gas conditions did not reach extreme pressures or temperatures, and we employed the ideal gas equation of state to recast state 2 in terms of observable quantities,

$$\Delta H_{\mathrm{sens}} = \frac{C_{\mathrm{p}2}}{R} P_2 V_2 - \frac{C_{\mathrm{p}1}}{R} P_1 V_1. \tag{5}$$

Inserting Eq. (5) into Eq. (3), and that result into Eq. (2), we found

$$\begin{aligned} Q &= \Delta H^0_{\mathrm{rxn}} + \Delta H_{\mathrm{pc}} + \frac{C_{\mathrm{p}2}}{R} P_2 V_2 - \frac{C_{\mathrm{p}1}}{R} P_1 V - P_2 V_2 - P_1 V_1 \\ &= \Delta H^0_{\mathrm{rxn}} + \Delta H_{\mathrm{pc}} + \frac{P_2 V_2}{\gamma - 1} - \frac{P_1 V_1}{\gamma - 1}, \end{aligned} \tag{6}$$

where P and V refer to the pressure and volume and γ is the ratio of specific heats of the gases considered. The last two terms on the right-hand side have been shown to represent energy stored in a pressure vessel. The PV term at state 1 represents energy in equilibrium with the environment outside the pressure vessel, and is therefore of no interest and is removed from the analysis. Solving for the unknown enthalpies yields

$$\Delta H^0_{\mathrm{rxn}} + \Delta H_{\mathrm{pc}} = \frac{P_2 V_2}{\gamma - 1} + Q. \tag{7}$$

This analysis cannot discriminate between the phase change and reaction enthalpies. However, this represents the energy liberated both in the form of heat and temporary gas production that together serve as the useful energy release of the MIC material. Fischer and Grubelich provided the theoretical enthalpies associated with reaction and phase change in the same way, and we have made useful comparisons to their reported values.[2]

Error sources and analysis

Three major sources of error affected this energy measurement scheme: uncertainty in heat loss, uncertainty in γ, and variations in weight or density from shot to shot. During the reaction time, energy was transferred to the surrounding gas by convection and radiation, and to the sample holder by conduction. The energy transferred to the gas appears as pressure on the transducers, but the sample holder absorbs the energy irreversibly on the time scale of interest. To ascertain the magnitude of error caused by this unknown heat loss, we have done a simple heat loss analysis according to the method described in Carslaw and Jeager for one-dimensional (Cartesian) heat transfer into a semi-infinite slab.[14] The assumption of planarity is reasonable based on the depth of heat penetration on the reaction time scale compared to the sample holder radius. We have observed no evidence of melting of the aluminum sample holder after many experiments, so we assumed that the temperature of the surface increased linearly from room temperature (RT) to 933 K (melting temperature of Al). The analysis showed a heat loss on the order of 2.5% using conservative assumptions. An error of +5% was thus assigned to account for the unknown heat loss to the sample holder. Note the + sign, indicating a bidirectional error of +/−2.5%. An obvious development for the calorimeter would be the addition of a low thermal conductivity sample holder material. To be conservative, we round this error up to +/−5%.

The uncertainty in the ratio of specific heats, γ, forms another potential source of error. For monatomic gases $\gamma = 1.67$, for water $\gamma = 1.01$, for diatomic gases $\gamma \sim 1.4$, and for tri- or polyatomic gases γ ranges from 0–1.4. Air contained in the vessel comprised the largest mole fraction at the end of the reaction at approximately 600 μmol. Experiments were performed using approximately 40 mg of the MIC material. If the MIC was formulated stoichiometrically with $WO_3 \cdot H_2O$, according to the computational thermochemical equilibrium code CHEETAH (Ref. 15) calculations, 110 μmol hydrogen gas was produced. If the MIC was formulated stoichiometrically with WO_3, Fischer and Grubelich reported the reaction produced 1430 μmol of gas per gram of WO_3/Al reaction, which resulted in approximately 60 μmol of reaction product gases in these experiments.

Assembling these values and using a mole-weighted average, we found that the value for γ was dominated by the value for air in the case of MIC formulated with WO_3, such that $\gamma = 1.40 \pm 0.04$. The uncertainty arises from the lack of knowledge regarding γ for the product gases. The magnitude

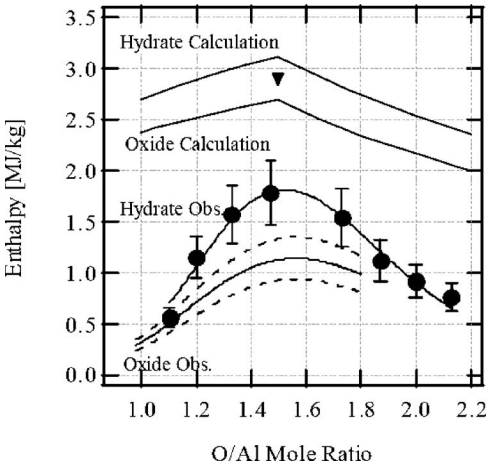

FIG. 5. The graph compares the observed energy release of the oxide MIC and the hydrate MIC. Also shown is the behavior predicted by thermodynamic calculations. The dashed lines bracketing the oxide observation show the overall error in those measurements, ±17%.

of the uncertainty was calculated using the mole fraction of product gases (10%) and a range of 1.0–1.8 for γ. For experiments conducted using $WO_3 \cdot H_2O$, the CHEETAH calculations indicated that hydrogen was the only major gas-phase product, for which $\gamma = 1.4$. The CHEETAH computational result was intuitively agreeable. However, we acknowledge the inherent uncertainty in such calculations and that deviations occurred for reactions that were not balanced. For this reason, we conservatively chose an error magnitude of 0.04, such that $\gamma = 1.40 \pm 0.04$ for the $WO_3 \cdot H_2O$ reaction. These error limits lead to an energy error of ±3% for typical peak pressures. Again, to be conservative, we round this error up to ±5%.

Shot-to-shot pressure variations produced the most significant source of scatter in the data. These variations may arise from variations in shot mass, different packing densities, and/or differing amounts of reactant consumed; however, the variation in shot mass was removed by normalizing the energy release to the mass of MIC used. To evaluate variations due to other uncertainties, we repeated each condition a number of times, usually five, and calculated an average and assigned 2σ as the error. In the current work, the error in energy ±15%.

We therefore find a total error of ±17%. It should be reiterated that the performance variation of the MIC itself causes the most significant error (±15%). The combined error of the uncertainty in γ and heat loss amounts to ±7%. The latter number, 7%, then becomes the stated calorimeter accuracy over the range of our observations. Larger deviation from stoichiometric mixtures would require a more careful analysis.

Comparison of hydrate to oxide

We first discuss the total energy release characteristics of the two oxidizers, then the energy release rates. Figure 5 shows the energy release characteristics of the Al/WO_3 reaction as a function of O/Al molar ratios. The curve is a best fit to the data presented in our previous work.[9] The nominal curve was calculated using $\gamma = 1.4$, as discussed in the previous section. The dashed lines represent a 17% error. The data points show the energy released from the $Al/WO_3 \cdot H_2O$ reaction, also using $\gamma = 1.4$. The graphs also show the calculated thermodynamic behavior of both oxide and hydrate reactions. The calculated energy release variations with stoichiometry for the WO_3 oxidized reaction and the $WO_3 \cdot H_2O$ oxidized reaction were calculated using the following reactions, respectively:

$$\mathrm{Al} + x\mathrm{WO_3} \rightarrow a\mathrm{Al} + b\mathrm{Al_2O_3} + c\mathrm{W} + d\mathrm{WO_3}, \tag{8}$$

$$\mathrm{Al} + x\mathrm{WO_3H_2O} \rightarrow a\mathrm{Al} + b\mathrm{Al_2O_3} + c\mathrm{H_2} + c\mathrm{W} + d\mathrm{WO_3H_2O}, \tag{9}$$

where x was varied to allow the O/Al molar ration to range from approximately 1.0–2.2. The other coefficients were then computed appropriately. The balanced (stoichiometric) reactions are

$$2\mathrm{Al} + \mathrm{WO_3} \rightarrow \mathrm{Al_2O_3} + \mathrm{W}, \tag{10}$$

$$8\mathrm{Al} + 3\mathrm{WO_3H_2O} \rightarrow 4\mathrm{Al_2O_3} + 3\mathrm{W} + 3\mathrm{H_2}. \tag{11}$$

The standard enthalpies of formation of the reaction constituents were used.[16] Phase changes were not included in the calculation, and those enthalpies account for approximately 8% of the total energy released in the oxide reaction, as illustrated by the stoichiometric value reported by Fischer and Grubelich[2] (which includes phase change) and shown in Fig. 5 for the oxide by the inverted triangle symbol. The reactions, as written, show our assumption for these calculations that the WO_3 and $WO_3 \cdot H_2O$ molecules either completely reacted or did not react at all. For example the W atom either was fully reduced or was in the 3+ oxidation state. We acknowledge that this was an oversimplification: the partially reduced W atom may form several lower oxides and excess hydrate will dissociate, producing free water in this system. However, the thermodynamic calculations were intended for a general comparison and showed that the hydrate system possesses a higher energy density than the oxide system. Further, Eq. (1) indicates that three additional moles of gas were formed during the reaction. MIC reactions typically do not produce permanent gas, but many formulations produce a temporary gas in the form of vaporized products, which play a role in reaction propagation and in exerting a force on the surroundings. The hydrogen produced by the hydrate reaction brings the total gas production to 0.76 mol of gas per 100 g of reactant, as compared to 0.14 mol/g for the oxide reaction. This is larger than any value for molar gas production in the list of binary reactions tabulated by Fischer and Grubelich.[2] Permanent gas formation has the additional advantage of the ability to perform *net* work on the surroundings, a feature lacking in most binary MIC systems. These experiments cannot provide information about afterburning of H_2. However, afterburn likely occurs under some circumstances.

Thermodynamic calculations are ignorant of transport and kinetic issues, and these processes contributed to the observed energy deficiency at the stoichiometric ratio. The physical explanation lies in the fact that the speed of the

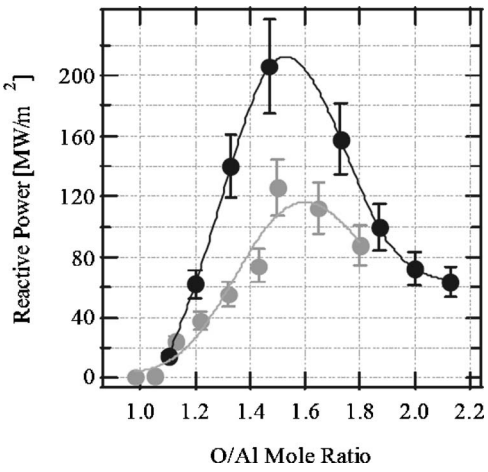

FIG. 6. Reactive power of the hydrate based MIC (dark lines) compared to the oxide MIC (light lines).

combustion propagation did not keep up with the material motion, and reactants were dispersed and/or quenched before all reactants were consumed.

Several observations support the hydrate reaction proceeding, as shown in Eq. (11). Most importantly, the energy release as a function of stoichiometry was consistent with the reaction as written. Also, as mentioned in the previous section, CHEETAH (Ref. 15) (equilibrium thermodynamics) finds H_2 as the only significant gas-phase product. In addition, as shown by the TGA data in Fig. 4, the hydrate liberates water at a temperature near 200 °C. Other researchers have observed[17] and we have also observed in our laboratory[18] that the direct combustion of Al and water to form hydrogen. The sum of this evidence strongly supports the three-component combustion of Al, WO_2, and water, as represented by Eq. (11).

Figure 6 compares the energy release rate of the $Al/WO_3 \cdot H_2O$ MIC to the Al/WO_3. The hydrate MIC produces energy at a rate on the order of 200 GW/m^2 at O/Al=1.5. This power level exceeded that of the oxide MIC by about the same amount as the energy density, suggesting that the hydrogen gas did appear to play a significant role in convective reaction propagation; however, the mode of reaction propagation is currently debated in the community. The experiments discussed here were not adequate to draw definitive conclusions about the reaction propagation mechanism.

CONCLUSIONS

We have formulated MIC materials from Al $+WO_3 \cdot H_2O$ and $Al+WO_3$. In order to characterize and compare the performance of these energetic materials, we have performed a first law analysis on the reaction of the energetic material in a constant volume vessel in which we can accurately measure the pressure at high pressurization rates. The analysis allowed the determination of total enthalpy change, the energy release rate, and the uncertainty in the measurement. The performance of the two MICs formulated with different oxidizers could then be reliably compared. We found that the hydrate oxidizer formulation had significantly higher reaction enthalpy and power at a stoichiometric O/Al ratio of 1.5 than the oxide formulation. The hydrate formulation produced approximately 1.8 MJ/kg compared to around 1.1 MJ/kg for the oxide, around 215 GW/m^2 for the hydrate, and approximately 130 GW/m^2 for the oxide. The behavior of the reaction over a range of $Al/WO_3 \cdot H_2O$ mixture ratios indicated that the aluminum reduced both WO_3 and H_2O, producing hydrogen gas and W metal. This conclusion was supported by other researchers who have investigated the direct combustion of aluminum by water.[17,18] Further, CHEETAH calculations also support this conclusion. The hydrogen gas formation has the additional advantage of the ability to perform net work on the surroundings, making the hydrate material a potential candidate for applications that require net gas production. Finally, the results presented here indicate that the $Al/WO_3 \cdot H_2O$ system is a high-performance formulation suitable for use in primers, electric matches, and explosive applications.

ACKNOWLEDGMENTS

Los Alamos National Laboratory is operated under the U.S. Department of Energy Contract No. W-7405-ENG-36. Funding was provided by the Defense Threat Reduction Agency. The authors thank Christopher Bulian, Zane Arp, James Busse, and Robert Dye for their contributions to this work.

[1] C. E. Aumann, G. L. Skofronick, and J. A. Martin, J. Vac. Sci. Technol. B **13**(3), 1178–1183 (1995).
[2] S. H. Fischer and M. C. Grubelich, Conference: International Pyrotechnics Seminar, Monterey, CA, 27–31 July 1998 (ISI Conf. No. 117083).
[3] P. W. Cooper, *Explosives Engineering* (Wiley-VCH, Weinheim, 1996).
[4] M. F. Gogulya, M. N. Makhov, M. A. Brazhnikov, and A. Yu. Dolgoborodov, *Energetic Materials: Structures and Properties*, 35th International Annual Conference of ICT, Karlsruhe, Federal Republic of Germany, 29 June–2 July, 79-1 to 79-1 (2004).
[5] G. P. Dixson, J. A. Martin, and D. Thomson, U.S. Patent No. 5,717,159 (10 February 1998).
[6] D. L. Naud, M. A. Hiskey, S. F. Son, J. R. Busse, and K. Kosanke, Journal of Pyrotechnics **17**, 65–75 (2003).
[7] P. Brousseau and C. J. Anderson, Propellants, Explos., Pyrotech. **27**, 300 (2002).
[8] K.-Y. Lee, J. Kennedy, B. Asay, S. F. Son, and E. S. Martin, *Shock Compression of Condensed Matter-2000*, edited by M. D. Furnish, Y. M. Guptam, and J. W. Forbes, American Institute of Physics Conference Proceedings (AIP, Melville, NY, 2003), p. 855.
[9] W. L. Perry, B. L. Smith, C. J. Bulian, J. R. Busse, C. S. Macomber, R. C. Dye, and S. F. Son, Propellants, Explos., Pyrotech. **29**, 99 (2004).
[10] Joint Committee on Powder Diffraction Standards Powder Diffraction File, International Center for Diffraction Data File No. 43-0679 (unpublished).
[11] M. Gotic, M. Ivanda, S. Popovic, and S. Music, Mater. Sci. Eng., B **B77**, 193 (2000).
[12] J. T. Mang, C. B. Skidmore, P. M. Howe, and R. P. Hjelm, AIP Conf. Proc. **505**, 699 (2000).
[13] O. Glatter and O. Kratky, *Small-Angle X-ray Scattering* (Academic, London, 1982).
[14] H. S. Carslaw and J. C. Jeager, *Conduction of Heat in Solids*, 2nd ed. (Clarendon, Oxford, UK, 1992).
[15] L. E. Fried, K. R. Glaesemann, W. M. Howard, P. C. Souers, and P. A. Vitello, CHEETAH 4.0; Lawrence Livermore National Laboratory Report No. UCRL-CODE-155944 (unpublished).
[16] R. C. Weast, *CRC Handbook of Chemistry and Physics*, 68th ed. (CRC, Boca Raton, FL, 1988).
[17] A. Ingenito and C. Bruno, J. Propul. Power **20**, 6 (2004).
[18] G. A. Risha, S. F. Son, R. A. Yetter, V. Yang, and B. C. Tappan, Proc. Combust. Inst. **31**, 2029–2036 (2007).